Rare Metal Materials and Engineering
Volume 51, Issue 6, June 2022
Available online at www.rmme.ac.cn

Science Press

Cite this article as: Shang Shiguang, Guo Xiongxiong, Ren Wei, et al. Hydrothermal Synthesis and Photovoltaic Performance of ZnO Nanorod Arrays for Silicon-based Heterojunction Solar Cell[J]. Rare Metal Materials and Engineering, 2022, 51(06): 1993-1998.

ARTICLE

Hydrothermal Synthesis and Photovoltaic Performance of ZnO Nanorod Arrays for Silicon-based Heterojunction Solar Cell

Shang Shiguang[1], Guo Xiongxiong[1], Ren Wei[1], Ju Xiaobao[2], Liu Youyao[1]

[1] School of Electronic Engineering, Xi'an University of Posts and Telecommunications, Xi'an 710121, China; [2] Xi'an Huanghe Photovoltaic Technology Co., Ltd, Xi'an 710000, China

Abstract: Heterojunction solar cells (HSCs) with the structure of p-Si/n-ZnO nanorod (NR) arrays were prepared by synthesizing a ZnO NR array film on patterned p-type silicon substrate through a low temperature hydrothermal method. ITO and Al films as the front and back contact electrode layers were deposited by DC-magnetron sputtering, respectively. The influences of various factors, such as annealing temperature for seed layer and hydrothermal synthesis time for ZnO NR arrays, on the crystal structure, surface morphology, and optical property of the ZnO NR array film were investigated. Results show that the optimized short-circuit current density and allover energy conversion efficiency of the p-Si/n-ZnO nanorod array HSCs are 11.475 $mA \cdot cm^{-2}$ and 2.0%, respectively. Compared with those of p-Si/n-thin film ZnO solar cell, the photovoltaic properties of the p-Si/n-ZnO nanorod array HSCs are improved significantly.

Key words: heterojunction solar cells; photovoltaic performance; ZnO nanorod arrays; conversion efficiency

Zinc oxide (ZnO) has excellent properties and extensive applications due to its wide direct band gap of 3.37 eV and high exciton binding energy of 60 meV[1]. To fulfill the performance requirements of novel devices, ZnO has been made into various nanomaterials, including nanoparticles[2], nanorods (NRs) [3-6], nanowires[7], nanoflowers[8], and nanowalls[9]. Among them, one-dimensional ZnO NR arrays have a large specific surface area, high light trapping effect and good directional electron conductivity[10], which can effectively increase the absorption rate of ultraviolet light and increase the generation rate of photo-generated carriers, and also reduce the recombination probability of photo-generated carriers. Thus they are ideal materials for preparing novel devices, such as humidity sensor[11], gas sensors[12,13], dye-sensitized solar cells[14,15], field emission electron beam sources[16], and ultraviolet photodetector[17]. In order to improve the performances, a variety of heterojunction devices have been developed due to their advantageous features. As previously reported, ZnO nanorod arrays/Si (GaN, NiO) heterojunction photodetector has reproducible results and fast recovery time[18-20]. And ZnO nanorod arrays/CuO (g-C_3N_4, BiOI) heterojunction[21-23] enhances photoelectrochemical performance. But, there are few reports on ZnO NR array HSCs.

In this study, a novel design of p-Si/n-ZnO NR array HSCs was proposed due to the following reasons. (1) ZnO NR arrays grown as the front layer of HSCs function as the antireflective layer to reduce the reflectivity of incidence sunlight and thus improving the utilizing efficiency of the incidence light[24-27]. (2) ZnO material may help extend the absorbed solar spectrum from visible light to ultraviolet light due to its much larger energy bandgap than Si's[10]. The fabrication procedure of p-Si/n-ZnO NR array HSCs was described, and their performance and the enhanced mechanism were discussed.

1 Experiment

Fig. 1 shows the fabrication procedure of the p-Si (100)/n-ZnO NR array HSCs. In Fig.1a~1d, in order to obtain ohmic

Received date: June 06, 2021
Foundation item: National Natural Science Foundation of China (61874087, 61634004)
Corresponding author: Shang Shiguang, Ph. D., Associate Professor, School of Electronic Engineering, Xi'an University of Posts and Telecommunications, Xi'an 710121, P. R. China, Tel: 0086-29-88166282, E-mail: shangshiguang05@163.com

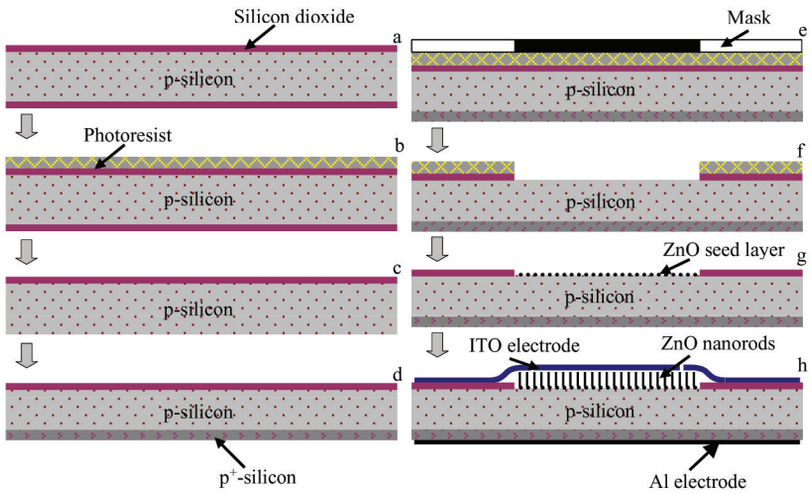

Fig.1 Schematic diagrams of the fabrication procedure for p-Si/n-ZnO nanorod array HSCs

contact (below 0.028 Ω/sq) between silicon substrate (with a resistivity of 1~5 Ω·cm) and Al metal electrode, the rear surface of Si substrate was heavily doped with boron by following typical semiconductor manufacturing processing: oxidation and photolithography, etching and thermal diffusion. Then, a thin layer of the photoresist was spin-coated on SiO_2/p-type silicon substrate, and a shadow mask with a special pattern was consequently placed on the surface of photoresist, and irradiated by UV light, as shown in Fig.1e. The patterned photoresist and SiO_2 layer with an active area 0.5 cm×0.5 cm were obtained by development and wet-etching processing in Fig. 1f. After the p-type silicon substrate was sequentially rinsed with deionization water, and dried with nitrogen purge, a ZnO seed layer was RF-sputtered on the p-type Si surface with the patterned photoresist and SiO_2 layer at room temperature (RT), and the patterned ZnO seed layer was obtained by stripping photoresist, as shown in Fig. 1g. After that, the ZnO seed layers were annealed at 250, 350, and 450 °C for 6 h to improve the crystalline quality of the seed layers for the subsequent NR growth. In Fig. 1h, the ZnO NRs were grown by the following procedure: the aqueous solution containing equimolar (~0.05 mol) zinc acetate dehydrate ($Zn(CH_3COO)_2$) and hexamethylenetetramine ($C_6H_{12}N_4$) were dissolved in 50 mL deionization water and stirred at room temperature for 30 min to ensure a complete mixing of the chemical solution. The hydrothermal ZnO NR growth was carried out in a high pressure reaction kettle by immersing the ZnO seed layer/Si substrate in the mixed solutions and heating at 80 °C for 3 and 5 h. Particularly, the ZnO seed layer faced downwards and leaned at ~45° against the reaction kettle in order to achieve a minimum temperature gradient for NR array growth[13]. Then, the samples with ZnO NR arrays were taken out of the solution, rinsed with the deionized water, and dried with N_2 purge. ITO and Al films were DC sputtered on the front (n-ZnO NR arrays side) and back (p^+-type Si side) surfaces of the samples to form the ohmic contact, respectively. The main parameters during fabrication of the p-Si/n-ZnO NR array HSCs are listed in Table 1.

Table 1 Main parameters during p-Si/n-ZnO nanorod array HSCs fabrication process

Parameter	Oxidation	Deposition		
		Seed layer	Al	ITO
Temperature/°C	960	RT	RT	RT
Volume ratio of Ar/O_2	0/1	2/1	1/0	1/0
Pressure/Pa	In air	0.9	1.2	1.2
Gas flow/mL·min^{-1}	100	30	40	40
Time/min	90	10	15	15
Power/W	-	150 (RF)	100 (DC)	100 (DC)

The crystalline phases of the samples were characterized by small angle X-ray diffraction in Shimadzu diffractometer (XRD-6000, Japan) using Cu-Kα radiation line. The morphologies of the samples were investigated by field emission electron microscope (FESEM, JSM-6700F) operated at 5.0 kV and high-resolution transmission electron microscopy (HRTEM, JEOL, JEM-2010). The diffuse reflectance spectra (DRS) were measured at room temperature by UV-Vis-NIR spectrophotometer (PerkinElmer LAMBDA, 1050). The current-voltage curves of solar cells were obtained employing precision source/measure unit (Keysight, B2902A) under standard AM1.5 illumination (100 mW·cm^2) using a solar simulator (Abet Technologies Inc., 10500) equipped with a xenon arc light source.

2 Results and Discussion

2.1 Crystal structure of ZnO seed layers and NRs

Fig. 2 shows XRD patterns of the ZnO seed layers on Si substrates and the as-grown ZnO NR arrays on ZnO seed layer/Si substrates. All the peaks of ZnO NR arrays are located at 34.62°, 36.36°, 47.70°, 63.02°, and 68.20°, corresponding to the (002), (101), (102), (103), and (112) orientations, respectively, which are contributed to the typical hexagonal wurtzite structured ZnO (according to JCPDS card

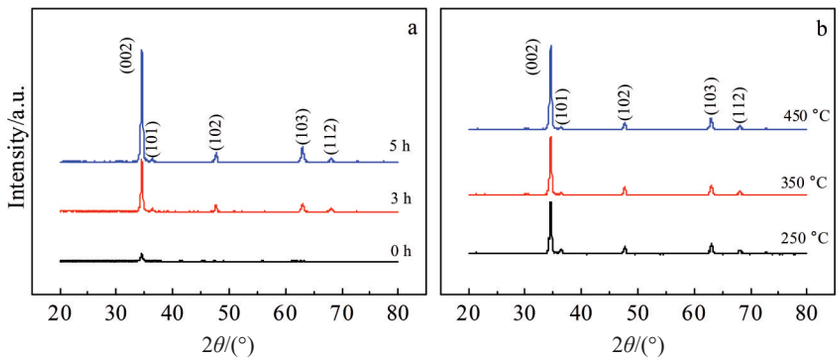

Fig.2 XRD patterns of ZnO seed layer annealed at 450 °C with the ZnO NR arrays growth for 0, 3 and 5 h (a) and the ZnO NR arrays grown on the ZnO seed layers annealed at 250, 350, and 450 °C for 5 h (b)

No. 36-1451). And no peaks from any other phase are observed. In Fig. 2a, only a small (002) peak from the ZnO seed layer (the 0 h curve) is observed, while five peaks appear with the (002) peak as the strongest one after the ZnO NR arrays start to grow for 3 h. When the ZnO NR arrays start to grow for 5 h, the (002) peak intensity increases much higher than that of other peak's intensity, which indicates that the ZnO NR arrays preferably grow with *c*-axis vertical to the silicon substrate and the crystalline quality of the seed layers also affects the growth of the ZnO NR arrays. In Fig. 2b, the intensity of (002) peaks of ZnO NR arrays becomes stronger and sharper with the annealing temperature of the seed layers increasing. This result is reasonable since the better crystalline quality of the ZnO seed layer will bring fewer defects where the ZnO NR will grow.

2.2 Microstructure of HSCs

Fig. 3 shows the FESEM micrographs of the ZnO seed layers with different annealing temperatures and the corresponding ZnO NR arrays grown on them for 3 and 5 h. In Fig.3a~3c, the surface morphology of the seed layer is clearly improved with the increase of annealing temperature. The surface of the seed layers at 250 °C (Fig. 3a) is composed of many small particles and there are many holes/defects randomly distributed on the surface. And the particle sizes at 350 (Fig.3b) and 450 °C (Fig.3c) become uniform and are ~25 and ~30 nm, respectively. In Fig. 3d~3i, the sample surface is densely filled with ZnO hexagonal NRs, the growth mechanism of this NR-shaped morphology is attributed to the substrate-induced oriental nucleation and fast growth under thermodynamic equilibrium state[28]. Fig. 3d~3f exhibit the morphology of ZnO NR arrays grown on Fig. 3a~3c for 3 h (marked sample 1~3), and the average diameters of ZnO NRs are 80, 90 and 120 nm, respectively. The corresponding diameters of ZnO NR arrays grown for 5 h (marked sample 4~6) are ~260, 270 and 350 nm, respectively. Compared with the insets in Fig.3i and Fig.3f, the length and verticality to the Si surface of ZnO NR arrays are enhanced with increasing the growth time. The results indicate that the surface density, diameter and length of the ZnO NRs strongly depend on the growth time of ZnO NR arrays and the seed layers to a certain extent.

Fig.4 reveals the TEM images of individual ZnO hexagonal NRs, which correspond to the sample in Fig.3e to confirm the detailed morphology and structure of FESEM image. The individual ZnO NRs are clearly seen in Fig. 4a and 4b with different low-resolution magnification scales. Particularly in Fig. 4b, the ZnO NR has a diameter of around 90 nm and an outer amorphous layer of ~7.8 nm in thickness. This outer layer is believed to be unreacted chemical, the mixture of $Zn(CH_3COO)_2$ and $C_6H_{12}N_4$, which can be removed by high temperature anneal processing[28]. The high resolution TEM image of the individual ZnO NR is shown in Fig. 4c, confirming not only the NR growth along the [002] direction (the lattice spacing of ~0.266 nm along the longitudinal axis direction), but also the high crystalline quality of it (according to the SAED pattern in Fig. 4d). The result is in good correlation with the XRD patterns in Fig.2.

Fig. 5 shows the FESEM images of ZnO NRs sputtering-coated with an ITO film from the top and cross-sectional view. Different from the isolated ZnO NRs in Fig.3i, the ZnO NRs in Fig. 5a have been connected with ITO film, which provides uninterrupted conduction paths to collect photon-generated electrons in HSCs. In Fig. 5b, the ZnO nanorods covered with ITO film change from uniform hexagonal rod to match rod shape, and their diameter is increased by ~50% from the bottom to the top. The inset in Fig. 5b further reveals that the "match head" of the ZnO NRs is close to a hemisphere and composed of many small ITO particles both on the top surface and on the side wall. It should be noted that the "match head" shape may help to focus the incidence sunlight into the ZnO NR and promote the sunlight absorption of the HSCs.

2.3 DRS of as-grown ZnO NR arrays

Fig. 6 shows the UV-Vis diffuse reflectance spectra (DRS) of as-grown ZnO NR arrays. For the samples 1~6, their averaged reflectance values are 49.8%, 26.6%, 37.7%, 27.7%, 21.1%, and 24.2% in the wavelength range of 200~1100 nm, respectively. In Fig. 6a, the absorption peak of samples 1~6 at room temperature is located at about 390, 389, 395, 388, 393, and 392 nm, respectively. The optical band gap (E_g), determined from the Kubelka-Munk mode, is calculated to be 3.18, 3.19, 3.14, 3.20, 3.16, and 3.16 eV, which are consistent with Ref. [29]. Compared with samples 1~3, the samples 4~6

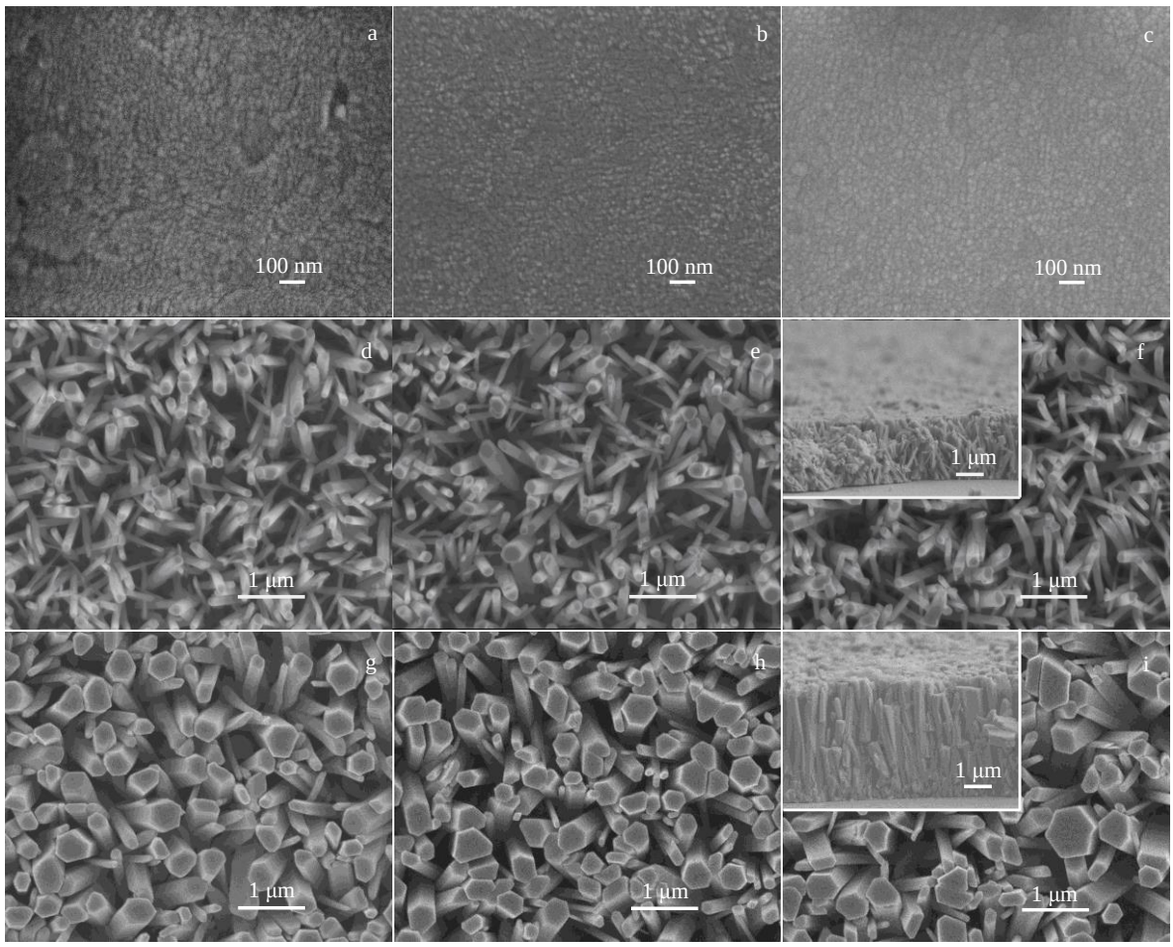

Fig.3 FESEM micrographs of the ZnO seed layers annealed at 250 ℃ (a), 350℃ (b), 450℃ (c), and corresponding ZnO nanorod arrays grown on them for 3 h (d~f) and 5 h (g~i), respectively

show a much lower reflectance in the wavelength range of 380~1100 nm, which indicates that the hydrothermal synthesis time can increase the absorption of the ZnO NR arrays for incidence light. The result in Fig. 6b shows that the averaged reflectance of samples decreases at first and then increases with increasing the annealing temperature for ZnO seed layer, and sample 5 has the lowest average reflectance of 21.1%. Another interesting point is that the reflectance ratio varies greatly, from 25% to 45% for samples 1~3, while it keeps relatively stable at ~20% for samples 4~6.

2.4 Photovoltaic performances of HSCs

Fig.7 plots the current-voltage curves of samples 1~6 covered with ITO front electrode and Al back electrode illuminated under a standard AM1.5 sunlight. As shown in Fig.7 (samples 1~3), the average short-circuits current density (J_{sc}) 10.591 mA·cm^{-2} and open-circuit voltage (V_{oc}) 0.327 V are observed. With increasing hydrothermal synthesis time, the average J_{sc} and V_{oc} values (samples 4~6) are 11.437 mA·cm^{-2} and 0.345 V. The results suggest a small increase in the average V_{oc} and J_{sc} for samples with increasing hydrothermal synthesis time.

The best stabilized conversion efficiency (η) of 2.0% (V_{oc}= 0.355 V, J_{sc}=11.475 mA·cm^{-2}, fill factor (FF) =0.499) was achieved with an area of 0.25 cm^2 without any antireflection coatings (sample 5). The allover energy conversion efficiency of p-Si/n-ZnO nanorod array HSCs is below the state of the silicon solar cell. The main reason is the presence of interface defect energy levels due to the difference of crystalline structure and lattice mismatch between the ZnO NRs and the Si substrate, which reduces the lifetime of the photogenerated carriers and increases its recombination rates. Compared with other thin-film ZnO/Si HSCs[30], the photovoltaic properties of the p-Si/n-ZnO nanorod array HSCs are enhanced significantly, which may provide useful information for potential application in future research.

3 Conclusions

1) A new solar cell model based on n-ZnO nanorod (NR) array film as front layer and p-type silicon as rear region is proposed. The ZnO nanorod array film can act as an active n-type layer as well as antireflection coating saving considerable processing cost.

2) The structure, morphology, and optical properties of the ZnO NR arrays strongly depend on the seed layer property resulted from thermal annealing temperature and the growth time of the ZnO NR arrays.

3) The ZnO NR arrays have a prominent wurtzite

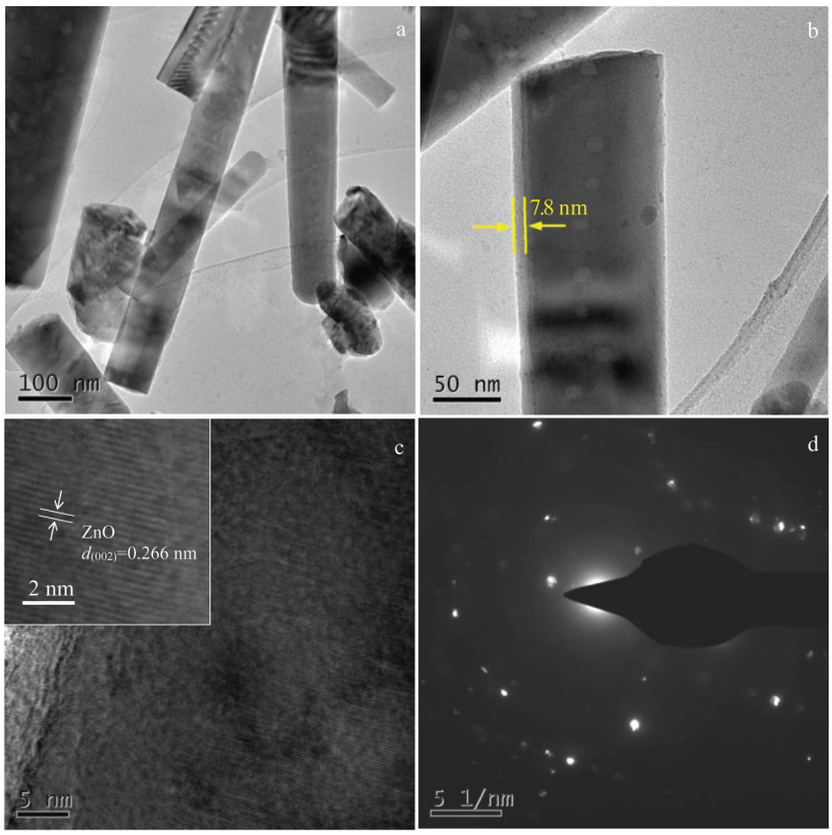

Fig.4 TEM images of ZnO NRs at low-resolution (a, b) and high resolution (c), and the corresponding SAED pattern (d)

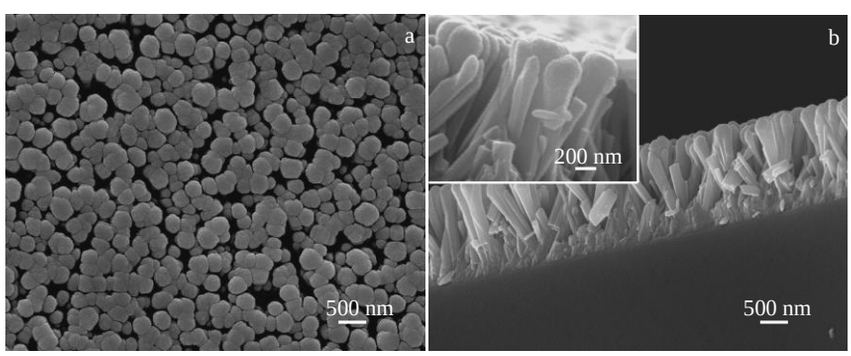

Fig.5 FESEM micrographs of ZnO NRs coated with ITO front electrode from top view (a) and cross sectional view (b)

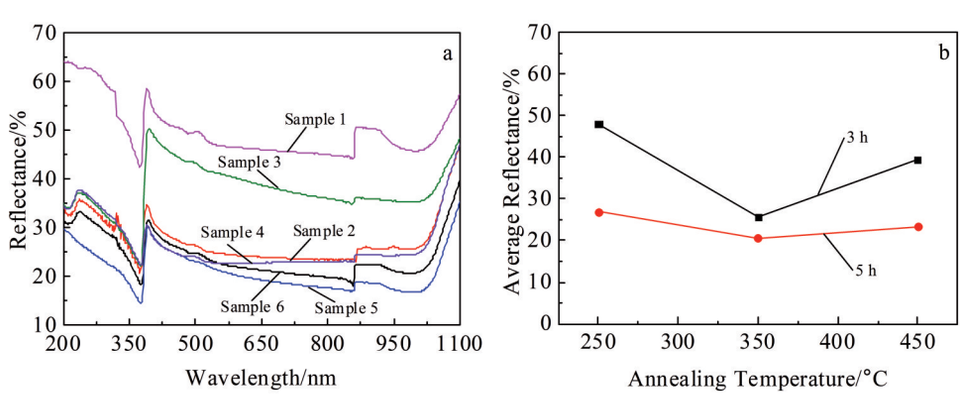

Fig.6 Diffuse reflectance spectra (DRS) of the as-grown ZnO nanorod arrays at room temperature (a), and the averaged reflectance variation with different annealing temperatures (b)

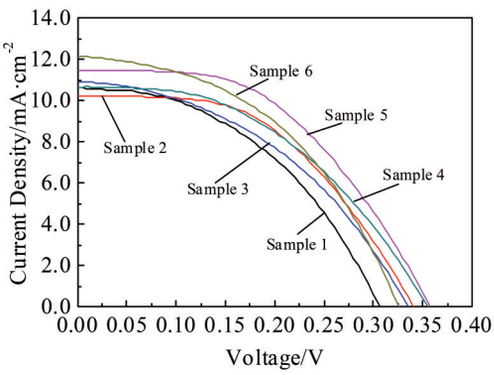

Fig.7 Current-voltage curves of samples 1~6 covered with ITO front electrode and Al back electrode under a standard AM1.5 illumination

hexagonal structure with preferred orientation along (002) polar surface. The average reflectance of samples decreases at first and then increases with increasing the seed layer annealing temperature.

4) The best conversion efficiency of the heterojunction solar cells is 2.0% with fill factor of 0.499.

References

1 Pourshaban E, Abdizadeh H, Golobostanfard M R. *Procedia Materials Science*[J], 2015, 11: 352
2 Zuo K, Blackman B R K, Williams J G *et al. Composites Science and Technology*[J], 2015, 113(5): 9
3 Shukla M, Pramila, Dixit T *et al. Applied Surface Science*[J], 2017, 422: 798
4 Saboor A, Shah M S. *Materials Science in Semiconductor Processing*[J], 2019, 93: 215
5 Hua Haoqiang, He Xinhua, Fu Xiaoyi *et al. Rare Metal Materials and Engineering*[J], 2018, 47(S2): 218 (in Chinese)
6 Li Yingying. *Rare Metal Materials and Engineering*[J], 2016, 45(1): 46
7 Demes T, Ternon C, Morisot F *et al. Applied Surface Science*[J], 2017, 410: 423
8 Umar A, Algarni H, Kim S H *et al. Ceramics International*[J], 2016, 42(11): 13 215
9 Islavath N, Das D, Joshi S V *et al. Materials & Design*[J], 2017, 116: 219
10 Bai Shouli, Chen Liangyuan, Li Dianqing *et al. Sensors and Actuators B: Chemical*[J], 2010, 146(1): 129
11 Jali M H, Rahim H R A, Johari M A M *et al. Optik*[J], 2021, 238: 166 715
12 Tao Dongliang, Liu Yanli, Jin Feng *et al. Rare Metal Materials and Engineering*[J], 2017, 46(9): 2720
13 Tan C H, Tan S T, Lee H B *et al. Sensors and Actuators B: Chemical*[J], 2017, 248: 140
14 Bai Te, Xie Yahong, Hu Jing *et al. Journal of Alloys and Compounds*[J], 2015, 644: 350
15 Gu Xiuquan, Qiang Yinghuai, Zhao Yulong. *Rare Metal Materials and Engineering*[J], 2014, 43(6): 1296
16 Su Xiaofeng, Chen Jianbiao, He Rumei *et al. Materials Science in Semiconductor Processing*[J], 2017, 67: 55
17 Zhang Dakuan, Sheng Yun, Wang Jianyu *et al. Optics Communications*[J], 2017, 395: 72
18 Ko K B, Ryu B D, Han M *et al. Journal of Alloys and Compounds*[J], 2020, 823: 153 884
19 Vikas L S, Vanaja K A, Subha P P *et al. Sensors and Actuators A: Physical*[J], 2016, 242: 116
20 Echresh A, Chey C O, Shoushtari M Z *et al. Journal of Alloys and Compounds*[J], 2015, 632: 165
21 Kumaresan N, Sinthiya M M A, Kumar M P *et al. Arabian Journal of Chemistry*[J], 2018, 13(1): 2826
22 Kumar P S, Selvakumar M, Babu S G *et al. Journal of Alloys and Compounds*[J], 2017, 701: 562
23 Zhang Chaojun, Fei Weihua, Wang Haoqing *et al. Journal of Hazardous Materials*[J], 2020, 399: 123 109
24 Kim K, Dhungel S K, Jung S *et al. Solar Energy Materials and Solar Cells*[J], 2008, 92(8): 960
25 Salman K A. *Solar Energy*[J], 2017, 147: 228
26 Qu Yazhou, Huang Xuan, Li Yanqiu *et al*. *Journal of Alloys and Compounds*[J], 2017, 698: 719
27 Bai Anqi, Tang Yang, Chen Jie. *Chemical Physics Letters*[J], 2015, 636: 134
28 Yang Weiguang, Wang Yali, Zhen Qiang *et al*. *Rare Metals*[J], 2011, 30(6): 676
29 Caglar Y, Ilican S, Caglar M. *Materials Science Poland*[J], 2017, 35(4): 824
30 He Bo, Ma Zhongquan, Xu Jing *et al. Materials Science in Semiconductor Processing*[J], 2009, 12(6): 248

硅基ZnO纳米棒阵列异质结太阳能电池的水热合成及其光伏性能

商世广[1]，郭雄雄[1]，任　卫[1]，巨小宝[2]，刘有耀[1]

(1. 西安邮电大学 电子工程学院，陕西 西安 710121)

(2. 黄河光伏科技股份有限公司，陕西 西安 710000)

摘　要：通过低温水热法，在图案化的p型硅衬底上合成氧化锌（ZnO）纳米棒阵列薄膜，制备出具有p-Si/n-ZnO纳米棒（NR）阵列结构的异质结太阳能电池（HSCs）。通过直流磁控溅射技术，分别在前后面板溅射沉积ITO和Al膜接触电极层。研究ZnO籽晶层的退火温度、ZnO纳米棒阵列水热合成的时间等因素对ZnO纳米棒阵列的晶体结构、表面形貌和光学性能的影响。p-Si/n-ZnO纳米棒阵列HSCs的最佳短路电流密度和总能量转换效率分别为11.475 mA·cm^{-2}和2.0%。相比p-Si/n-ZnO薄膜HSCs，p-Si/n-ZnO纳米棒阵列HSCs的光伏性能得到了有效提高。

关键词：异质结太阳能电池；光伏性能；ZnO纳米棒阵列；转换效率

作者简介：商世广，男，1975年生，博士，副教授，西安邮电大学电子工程学院，陕西 西安 710121，电话：029-88166282，E-mail：shangshiguang05@163.com